**Article ID:** 1003- 6326(2000)02- 0149- 07

# HREM study on stacking structure of SiGe/Si infrared detector①

LIU An-sheng(刘安生), LIU Zheng(刘 峥), SHAO Bei-ling(邵贝羚), WANG Jing(王 敬)
*General Research Institute for Nonferrous Metals, Beijing 100088, P. R. China*

**Abstract:** Stacking structure and defects in SiGe/P-Si infrared detector were studied by using localization high resolution electron microscopy (HREM). The photosensitive region in the detector consists of 3 $P^+$-$Si_{0.65}Ge_{0.35}$ layers and 2 UD-Si (undoped Si) layers. The interface between $Si_{0.65}Ge_{0.35}$ and UD-Si is not sharp and has a transition zone with non-uniform contrast. The misfit stress of interface is distributed gradiently along the normal direction of the interface. Therefore the crystal defects and serious lattice deformations on the interface have not been found. A defect area with a shape of inverted triangle exists in the edge of photosensitive region. The main types of the defects in the area are stacking faults and microtwins. The stacking faults are on $(\bar{1}\,\bar{1}\,1)$, and the thickness of the most microtwins is less than 4 interplanar spacing and the twin plane is $(\bar{1}\,\bar{1}\,1)$. The $Si_{0.65}Ge_{0.35}$ and UD-Si layers on amorphous $SiO_2$ layer consist of polycrystals grown by random nucleation, and are in wave.

**Key words:** heterogeneous interface; infrared detectors; high resolution electron microscopy(HREM)
**Document code:** A

## 1 INTRODUCTION

Infrared detectors and infrared focal plane arrays possess extensive and important applications in the fields of guidance, night-vision, remote sense, telemetry, early warning, surveillance of deep space, medical diagnose, etc. $P^+$-$Si_{1-x}Ge_x$/P-Si heterojunction internal photoemission (HIP) detector possesses the advantages of all kinds of detectors used at present, and can work at 3~ 5 μm and 8~ 14 μm two atmospheric windows. The quantum efficiency of HIP detector is higher than that of silicide Schottky-barrier detector and its response wavelength can be adjusted. Besides, it is easy to form monolithic integration with CMOS or CCD reading circuit and the cost is low. Therefore, it has attracted a great attention recently.

In 1990, for the first time, Lin et al[1] prepared $P^+$-$Si_{1-x}Ge_x$/P-Si HIP infrared detector with 2~ 10 μm response range and 1% quantum efficiency. In 1991, Tsaur et al[2] successfully developed $P^+$-$Si_{1-x}Ge_x$/P-Si HIP long-wavelength infrared detector arrays with 400 × 400 pixel and achieved monolithic integration with CCD reading circuit. For the infrared detector arrays, cut-off wavelength is 9.3 μm, response nonuniformity is less than 1% and minimum resolvable temperature is less than 0.2 K. In 1993, State Key Lab for Applied Surface Physics in Fudan University of China also prepared $P^+$-$Si_{1-x}Ge_x$/P-Si HIP infrared detector. Its cut-off wavelength is 9 μm. At 52 K, the detectivity for 500 K blackbody $D^*_{500\,K} = 2.0 \times 10^8$ cmHz$^{1/2}$/W[3,4].

In 1997, Wang et al[5~7] developed P+-$Si_{0.65}Ge_{0.35}$/P-Si HIP infrared detector with a high quantum efficiency. The performance of the unbiased detector at 77 K has been improved to $D^*$ (5.5, 1000, 1) = $1.1 \times 10^{10}$ cmHz$^{1/2}$/W. The peak quantum efficiency has reached 4% and the response range is 2~ 8 μm. The detector at 77 K shows ideal diode characteristics. The back leakage current density is only $10^{-4}$ A/cm$^2$.

It is well known that the properties of the detectors are dependent on their microstructures. The microstructures of the HIP infrared detector were studied using several electron microscopies[8~10]. But the interface structure and defects in the detectors can be only identified by high resolution electron microscopy (HREM). In this paper, the experimental results about interface structure and defects in the detector, which was studied at atomic level, will be presented.

## 2 EXPERIMENTAL

Both studies of Park et al[11] and Wang et al[5] indicated that using stacking structure as an emitter and making each $Si_{1-x}Ge_x$ layer thinner, the infrared detector will possess higher transport efficiency, and the quantum efficiency of the detector is raised. For this reason, on the P-Si substrate, 3 $P^+$-$Si_{0.65}Ge_{0.35}$ layers were locally grown and separated by undoped Si (UD-Si) layers by using molecular beam epitaxy (MBE) technique, as shown in Fig. 1. The design thickness of each $Si_{0.65}Ge_{0.35}$ and UD-Si layers is 6 nm and 50 nm, respectively. The function of $P^+$ region shown in the left side in Fig. 1 is to form a good Ohm contact between aluminum electrode and Si Sub-

① **Foundation item:** Project 69576002 supported by the National Natural Science Foundation of China
**Received date:** Dec. 4, 1998; **accepted date:** May. 4, 1999

strate. It is considered that the defects existed in $Si_{0.65}Ge_{0.35}$ and UD-Si layers at the edge of photosensitive region will cause leakage of electricity. An $N^+$ zone as a protection ring was prepared to decrease the leakage in the edge.

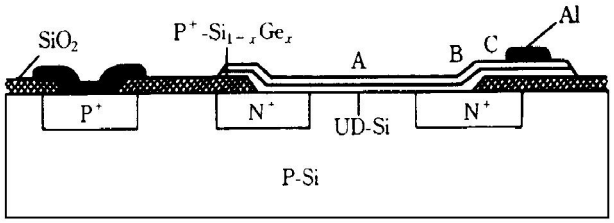


**Fig. 1** Cross-section schematic of $P^+$-$Si_{0.65}Ge_{0.35}$/P-Si HIP infrared detector with a stacked structure

For studying the stacking structures and defects of the detectors, diffraction contrast images and high resolution images of localization cross-section specimens were observed. The wafers with devices were adhered face to face with G1 type epoxy resin, according to marking location in advance. This pair of wafers were cut at the appoint position by means of a low speed saw to make the slices including a detector. The slices were mechanically ground to a thickness of 20 μm by diamond powder cream and then thinned to just penetration by using ion milling instrument of Gatan 600. The ion milling current is 0.5 mA, the accelerating voltage is 5 kV, and the incident angle of ion beam is 15°~ 12°. To study the effects of microstructure on properties, the observation will center on typical A, B and C regions shown in Fig. 1. For the observation of diffraction contrast image and high resolution image, JEM-2000FX and JEM-2010 transmission electron microscopes were used at operating voltage of 200 kV.

## 3 RESULTS AND DISCUSSION

Fig. 2 shows a cross-section image of stacking structure of the photosensitive region and polycrystal region on $SiO_2$ layer (A and C regions, as shown in Fig. 1) in the infrared detector. It can be seen from Fig. 2 that the surface of P-Si substrate is flat and smooth. The corresponding electron diffraction pattern indicates that the normal direction of photograph plane is [011] and orientation of P-Si substrate surface is [100]. Any crystal defect has not been found in the P-Si substrate. When the specimen is tilted, the extinction fringes caused by local bending of film during preparing TEM specimen can be seen. In photosensitive region, $Si_{0.65}Ge_{0.35}$ layer appears black line and the UD-Si layer as well as P-Si substrate is gray under this imaging condition.

Fig. 3 shows the high resolution image of a small segment of $P^+$-$Si_{0.65}Ge_{0.35}$/UD-Si layers and P-Si substrate in A region. It is impossible and unnecessary to entirely show the image of the whole stacking structure under 2 000 000 magnification. We have to

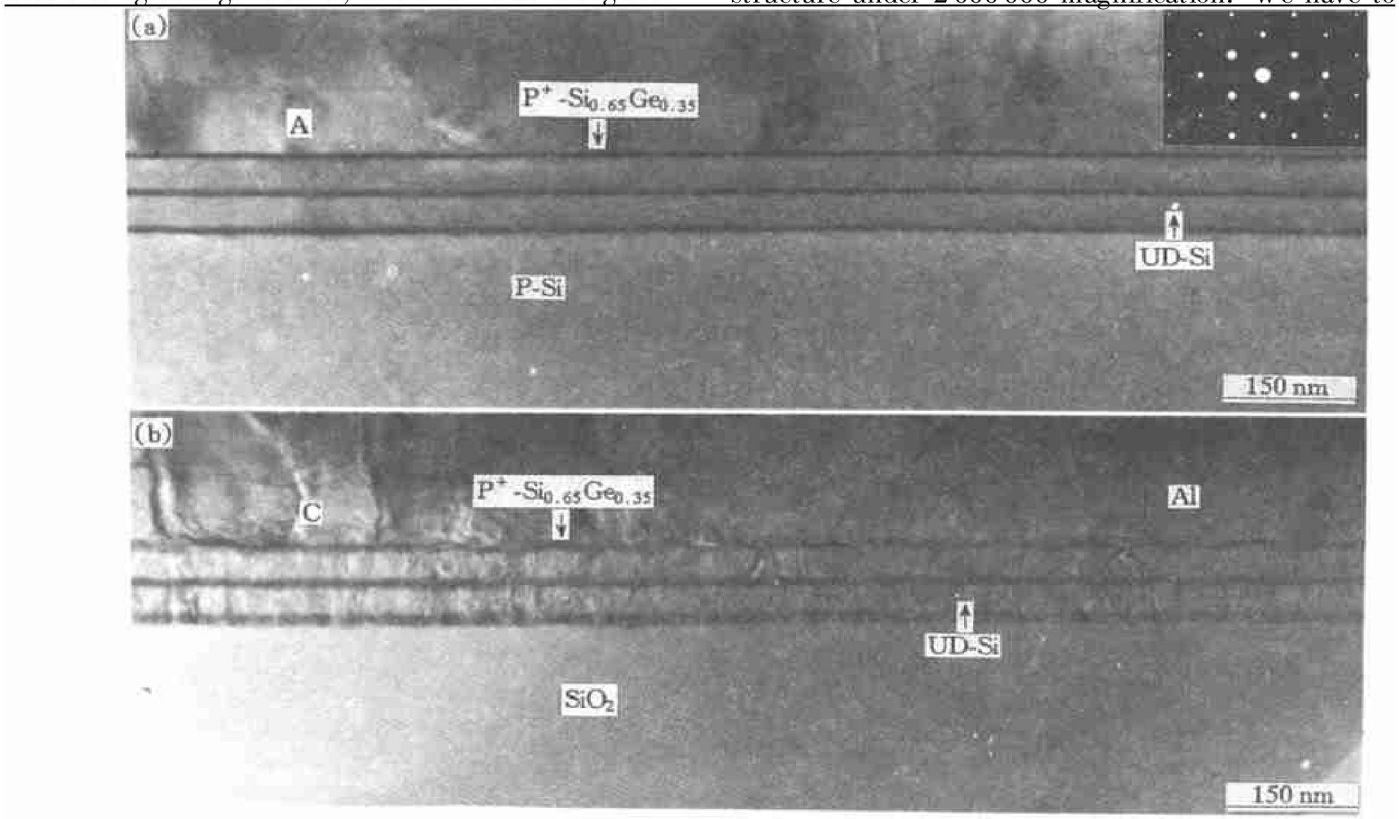


**Fig. 2** Cross-section image of stacking structure of photosensitive region and polycrystal region on $SiO_2$ layer in infrared detector

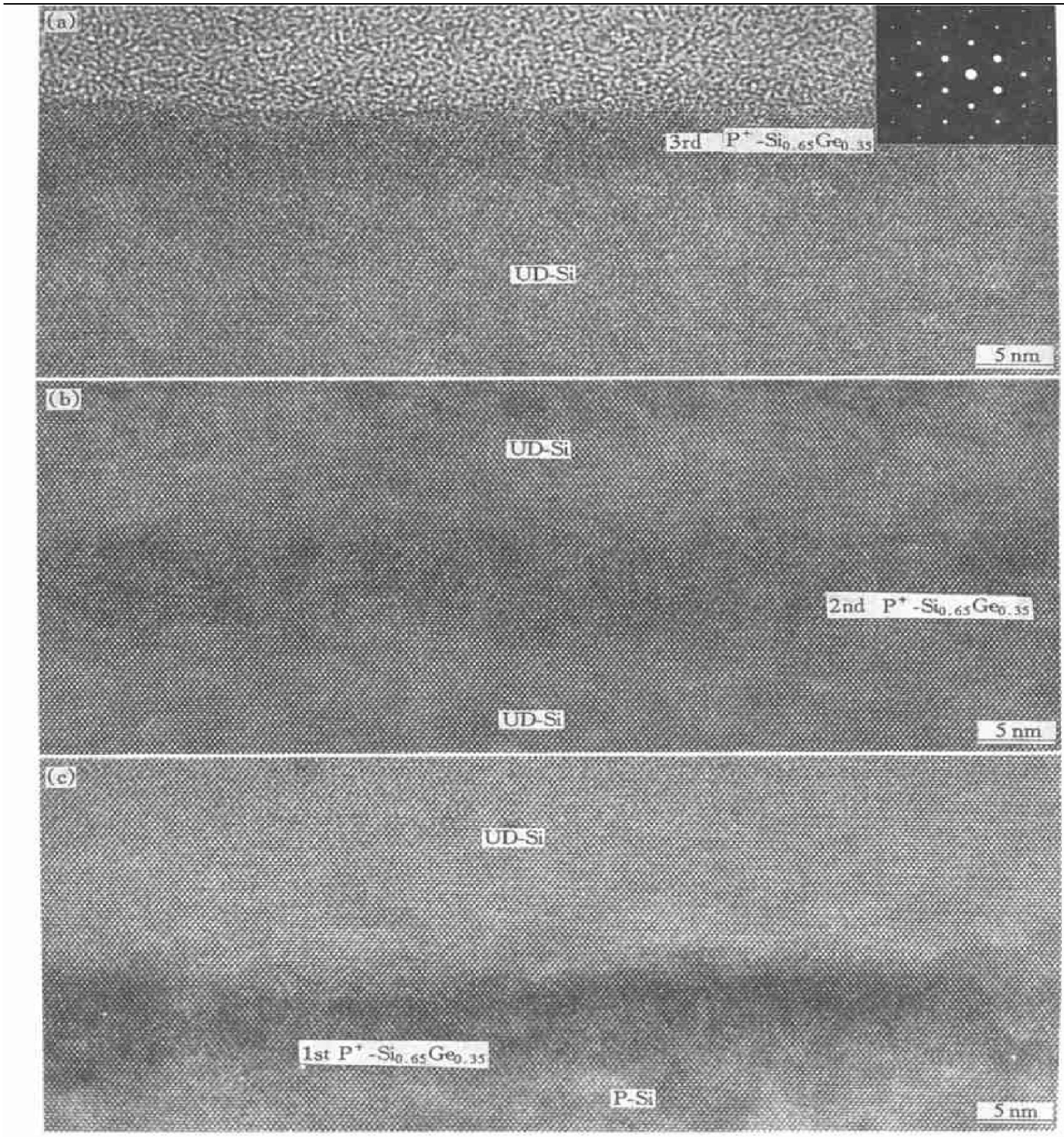


**Fig. 3** HREM image of $P^+$-$Si_{0.65}Ge_{0.35}$/UD-Si layers in photosensitive region (*A* region)

cut off a part of the image of UD-Si layer, and show the high resolution images of three $Si_{0.65}Ge_{0.35}$ layers and the areas near the interfaces, as shown in Fig. 3. Because Ge atom is heavier than Si atom, the lateral ribbons with dark gray contrast in high resolution image are $Si_{0.65}Ge_{0.35}$ layers, and the areas with light gray is UD-Si layers, and the bottom area in Fig. 3 (c) is the P-Si substrate. It can be seen in Fig. 3 that $P^+$-$Si_{0.65}Ge_{0.35}$/UD-Si and $P^+$-$Si_{0.65}$-$Ge_{0.35}$/P-Si interfaces are not sharp and have a transition zone with non-uniform contrast. If the layers are divided along the middle line of the transition zone, the thickness of $Si_{0.65}Ge_{0.35}$ layer is about 7 nm, and the thickness of UD-Si layer is about 56 nm. Epitaxy temperature of $Si_{0.65}Ge_{0.35}$ and UD-Si layers is only 650 ℃. The temperature of followed treatment does not exceed the epitaxial temperature. But Ge atoms in $Si_{0.65}Ge_{0.35}$ layers still diffuse into UD-Si layers and P-Si substrate. Under the effect of stress field caused by mismatch between $Si_{0.65}Ge_{0.35}$ and Si layers, the diffusion of Ge atoms appears non-uniform and the non-uniform contrast mentioned above is formed. The out-diffusion of Ge atoms will raise the leakage current of the infrared detector. The experiments[7] indicate that if the specimen is annealed at 1000 ℃ for 10 s after epitaxis, severe out-diffusion of Ge atoms ap-

pears, and the $Si_{0.65}Ge_{0.35}$ layer changes qualitatively, and the properties of the device degenerate and even fail. Although the mismatch of $Si_{0.65}Ge_{0.35}$/Si interface is 2.1%, none of lattice defect and serious lattice deformation have been found, except the edge of photosensitive region. This reason may be that the diffusion of Ge atoms has relaxed the mismatch stress and makes the stress gradually distributed along the normal direction of the interface.

From diffraction contrast image it can be seen that the image of $Si_{0.65}Ge_{0.35}$ layer curves near the border of photosensitive region, as shown in Fig. 4 (a). It is known from high resolution image in Fig. 4 (b) that $Si_{0.65}Ge_{0.35}$/UD-Si layer on the slope at the edge of amorphous $SiO_2$ layer is polycrystalline. Even though $Si_{0.65}Ge_{0.35}$/UD-Si layer at the edge of photosensitive region grows on the single crystal P-Si substrate, it is still affected by adjacent polycrystal layer grown simultaneously on the slope of amorphous $SiO_2$ layer, and the defects are caused in the side of

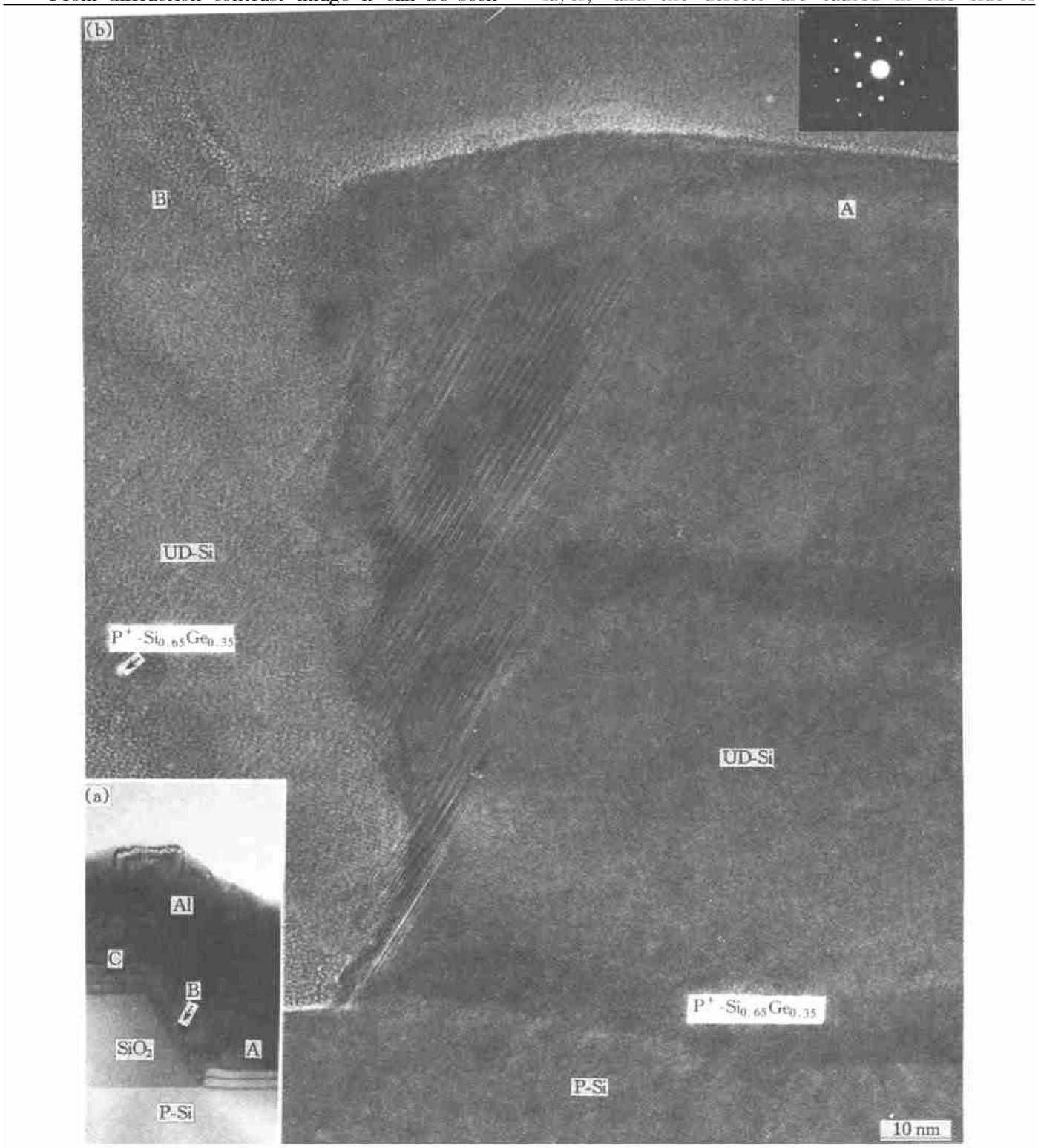


**Fig. 4** Multilayer structure image at the slope (B region) of amorphous $SiO_2$ step (a) and HREM image of bordering area between A and B regions (b)

photosensitive region. The defect area is smaller in initial epitaxis and is growing larger and larger with epitaxis and finally appears in a shape of inverse triangle. The width of the defect area in the final epitaxial layer is about 42 nm. The incidence direction of electron beam in Fig. 4(b) is [011]. It is indicated from the analysis that the main defects are stacking faults and microtwins. The stacking faults are on the $(\bar{1}\,\bar{1}\,1)$ plane. The twinning plane is $(\bar{1}\,\bar{1}\,1)$ and the thickness of the most microtwins is less than 4 interplanar spacing. It is obvious that the edge of photosensitive region has not ideal perfect crystal structure. For technology, it is very difficult to avoid producing defects in the border area between monocrystal region and polycrystal region during growth, but it is possible to reduce the defect area. These defects may cause electricity leakage. In order to decrease the leakage, an $N^+$ zone as a protection ring has been prepared inside the P-Si substrate near the edge of photosensitive region, as shown in Fig. 1. Although the doping in $N^+$ zone makes scattering factor of this zone different from other region of P-Si substrate, the effect on scattering of incidence electron beam is so weak that the image of $N^+$ zone can not be observed.

In the outer of photosensitive region, there is an amorphous $SiO_2$ layer with thickness of 410 nm, as an insulating layer. The slope of $SiO_2$ layer adjacent to photosensitive region has an angle of 58° with surface of P-Si substrate. The amorphous $SiO_2$ layer is prepared by using hot-oxidation technique. The interface between amorphous $SiO_2$ layer and P-Si substrate is flat and smooth, as shown in Fig. 5. The fluctuation of $SiO_2$/P-Si interface in [100] direction does not exceed 300% of interplanar spacing. It is known by comparing Fig. 3 with Fig. 5 that the $SiO_2$/P-Si interface is flatter than the interface of photosensitive region.

Fig. 6 shows the high resolution image of $Si_{0.65}Ge_{0.35}$/UD-Si stacking layers (C region) on insulating amorphous $SiO_2$ step. The high resolution images of three $Si_{0.65}Ge_{0.35}$ layers and the areas near the interfaces are shown in Fig. 6(a), (b) and (c), respectively. It can be seen that the surface of the amorphous $SiO_2$ layer is flat. $Si_{0.65}Ge_{0.35}$ and UD-Si layers both consist of polycrystals. The first $Si_{0.65}Ge_{0.35}$ layer grows on the surface of amorphous $SiO_2$, and the $Si_{0.65}Ge_{0.35}$ crystals nucleate randomly on the $SiO_2$ surface at the beginning of growth. Then the crystals of the layer grow epitaxially on these nuclei. Because the nuclei are close to one another, about 5~12 nm, and the grains interact on one another during growing, the growing direction of the grains changes when they grow to a certain degree. So columnar grains are not formed. Generally, the larger the grain, the longer the grain in growing direction. The followed UD-Si and $Si_{0.65}Ge_{0.35}$ layers grow in this way. The growing speed is different with different orientation, therefore $Si_{0.65}Ge_{0.35}$/UD-Si polycrystal layers with wavy shape are formed. It can be seen also that the first $Si_{0.65}Ge_{0.35}$ layer on the amorphous $SiO_2$ is thicker and lighter in contrast. It is indicated that the diffusion of Ge atoms in this layer is severer than that in the second and the third $Si_{0.65}Ge_{0.35}$ layers. This is related to higher temperature of $SiO_2$ surface comparing to that of P-Si surface and UD-Si layer surface due to poor thermal conductivity of $SiO_2$ layer during growing.

## 4 CONCLUSIONS

1) The photosensitive region of the detector

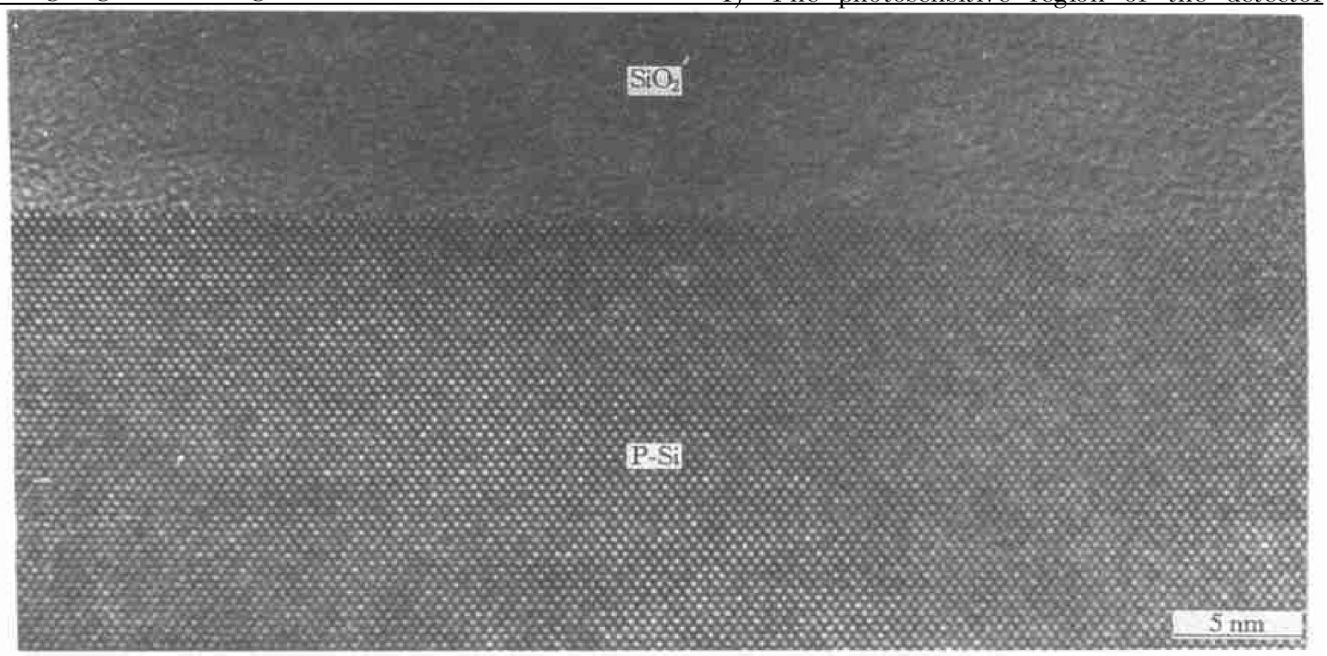


**Fig. 5** HREM image of amorphous $SiO_2$/P-Si interface

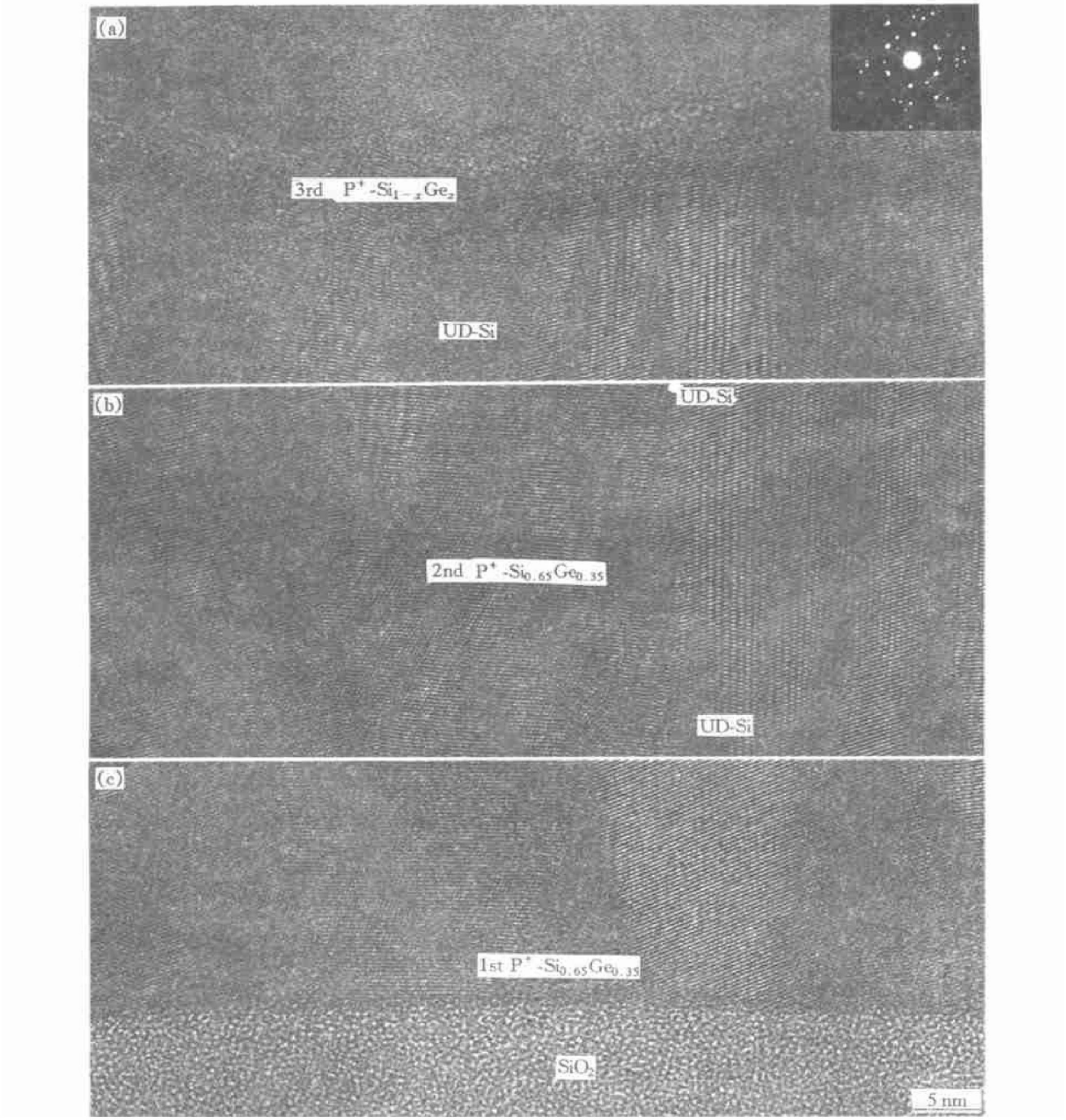


**Fig. 6** HREM image of multilayer Si0.65Ge0.35/UD-Si on amorphous $SiO_2$ layer

consists of 3 $P^+$-$Si_{0.65}Ge_{0.35}$ layers and 2 UD-Si layers. It is seen that the $Si_{0.65}Ge_{0.35}$ and UD-Si layers are flat and smooth in the low magnification image, but these layers are not really flat and fluctuate slightly in high resolution image. The $P^+$-$Si_{0.65}Ge_{0.35}$/UD-Si interfaces are not sharp and a transition zone caused by diffusion of Ge atoms exists. In the transition zone there is a gradual distribution of mismatch stress between layers along normal direction of the interface. Therefore, no any of crystal defect and serious lattice deformation at the interfaces has been found.

2) A defect area exists in the edge of photosensitive region. This area appears in shape of inverse triangle in cross-sectional view. The main defects are stacking faults and microtwins. The stacking faults are on the $(\bar{1}\,\bar{1}\,1)$ plane and the twining plane is $(\bar{1}\,\bar{1}\,1)$ too. The thickness of the most microtwins is less than 4 interplanar spacing.

3) $Si_{0.65}Ge_{0.35}$/UD-Si layers on $SiO_2$ layer consist of randomly grown grains. The columnar grains in the growing direction have not been formed. The growing speed is different with the different orientation of grains. The polycrystal $Si_{0.65}Ge_{0.35}$/UD-Si layers are in wave.

## ACKNOWLEDGEMENTS

The authors are thankful to Prof. Tsien Peixin and Dr. WANG Ruizhong (Institute of Microelectronics, Tsinghua University) for providing the specimens used in this study.

## REFERENCES

[1] Lin T L and Maserjian J. $Si_{1-x}Ge_x$/Si heterojunction photoemission long-wavelength infrared detectors [J]. Appl Phys Lett, 1990, 57(14): 1422~1424.

[2] Tsaur B Y, Chen C and Marino S. Long-wavelength $Si_{1-x}Ge_x$/Si heterojunction infrared detectors and 400×400-element image arrays [J]. IEEE Electron Device Letters, 1991, 12(6): 293~296.

[3] GONG Darwei, YANG Xiaoping and WEI Xing. A new $Ge_xSi_{1-x}$/Si heterojunction far-infrared detector [J]. Chinese Journal of Semiconductors, 1993, 14(4): 260~263.

[4] GONG Darwei, YANG Xiaoping and WEI Xing. 9 μm of $P^+$-$Ge_xSi_{1-x}$/P-Si heterojunction infrared detector [J]. Chinese Journal of Infrared and Millimetric Wave, 1994, 13(2): 149~152.

[5] WANG Ruizhong, CHENG Peiyi, Tsien Peixin, et al. Improvement of properties of $P^+$-$Ge_xSi_{1-x}$/P-Si HIP infrared detector [J]. Laser and Infrared, (in Chinese), 1997, 27(6): 362~365.

[6] WANG Ruizhong, CHENG Peiyi, Tsien Peixin, et al. Structure improvement and 77 K performance of $P^+$-$Ge_xSi_{1-x}$/P-Si heterojunction internal photoemission long-wavelength infrared detectors [J]. Chinese Journal of Semiconductors, 1997, 18(6): 636~640.

[7] WANG Ruizhong, CHENG Peiyi, Tsien Peixin, et al. Improvement of performance of $P^+$-$Ge_xSi_{1-x}$/P-Si heterojunction internal photoemission infrared detectors at 77 K [J]. Infrared Physics & Technology, 1998, 38: 293~296.

[8] LIU Ansheng, SHAO Berling, AN Sheng, et al. Applications of secondary electron composition contrast imaging method in microstructure studies on heterojunction semiconductor devices and multilayer materials [J]. Rare Metals, (in Chinese), 1998, 22(6): 401~406.

[9] LIU Ansheng, SHAO Berling, AN Sheng, et al. Investigation of microstructure of $P^+$-$Si_{1-x}Ge_x$/P-Si infrared detectors [J]. Journal of Chinese Electron Microscopy Society, 1998, 17(5): 535~539.

[10] LIU Ansheng, SHAO Berling, LIU Zheng, et al. TEM study on $P^+$-$Si_{0.65}Ge_{0.35}$/P-Si HIP infrared detector [J]. Trans of Nonferrous Met Soc China, 1999, 9(3): 481~486.

[11] Park J, Lin T L, Jones E, et al. Long-wavelength $Si_{1-x}Ge_x$/Si heterojunction internal photoemission infrared detectors [J]. SPIE, 1993, 2020: 12~21.

[12] CHENG Peiyi, WANG Ruizhong and Tsien Peixin. Raman spetrum analysis of composition and stress in $Ge_xSi_{1-x}$ film grown with MBE [A]. In QUE Duanlin ed. Proceedings of the 5th national solid film symposium [C], Fenghua, Zhejiang, China, 1996, 112~114.

**(Edited by HUANG Jinsong)**